Trajectory analysis of a soccer ball

John Eric Goff
Department of Physics, Lynchburg College, Lynchburg, Virginia 24501

Matt J. Carré
Department of Mechanical Engineering, University of Sheffield, Sheffield S1 3JD, United Kingdom

(Received 27 February 2009; accepted 16 July 2009)

We performed experiments in which a soccer ball was launched from a machine while two cameras recorded portions of its trajectory. Drag coefficients were obtained from range measurements for no-spin trajectories, for which the drag coefficient does not vary appreciably during the ball's flight. Lift coefficients were obtained from the trajectories immediately following the ball's launch, in which Reynolds number and spin parameter do not vary much. We obtain two values of the lift coefficient for spin parameters that had not been obtained previously. Our codes for analyzing the trajectories are freely available to educators and students.
[DOI: 10.1119/1.3197187]

I. INTRODUCTION

Of great interest to those who study the physics of sports are the aerodynamic properties of various objects. Seminal works by Briggs[1] on baseballs and Achenbach[2,3] on smooth and rough spheres have become standard references for those studying spherically shaped sports balls. Further work has been done on baseballs,[4,5] golf balls,[6] tennis balls,[7] and volleyballs.[8]

The understanding of the physics of soccer balls has increased greatly in the past decade and a half. Several wind-tunnel experiments[9–12] and computer models[13–17] have been done on the aerodynamics of soccer balls. Our contribution is on the analysis of trajectories. Similar studies have been performed on tennis balls[18,19] and baseballs.[20,21]

The most important number used to describe phenomena associated with soccer balls moving through air is the dimensionless Reynolds number, Re, defined as[22]

$$\mathrm{Re} = \frac{vD}{\nu}, \tag{1}$$

where v is the air speed far from the ball in the ball's rest frame, which is the speed of the ball in the stationary air's frame. Also D is the ball's diameter, and ν is the kinematic viscosity, defined as the ratio of the viscosity μ to the density of air ρ. For our experiments $\nu \simeq 1.54 \times 10^{-5}$ m^2/s. For $D \simeq 0.218$ m Eq. (1) becomes for a soccer ball moving through air

$$\mathrm{Re} \times 10^{-5} \simeq \frac{v}{7\ \mathrm{m/s}} \simeq \frac{v}{16\ \mathrm{mph}}. \tag{2}$$

The game of soccer is played mostly for 10 mph $< v <$ 70 mph (4.5 m/s $< v <$ 31 m/s), and hence the range of Reynolds numbers relevant for a soccer game is approximately 70 000 $<$ Re $<$ 490 000.

As the Reynolds number is increased through a critical value, air flow in the ball's boundary layer changes from laminar to turbulent flow. The boundary layer separates farther back on the ball, and the resistive drag coefficient drops.[23] Panel connections, like stitches on a baseball and dimples on a golf ball, induce turbulence at a Reynolds number lower than that of a smooth ball. One soccer ball wind-tunnel experiment yields[9] a transition from laminar to turbulent flow at Re $\simeq 1.4 \times 10^5$ (ball speed of about 9.9 m/s). Another study[10] found the transition to be slightly greater than Re $= 2 \times 10^5$ (ball speed of about 14 m/s). Not all soccer balls are the same. Although we studied a standard 32-panel stitched ball,[24] there are other types. The 2006 World Cup, for example, used a 14-panel thermally bonded ball.

If a player imparts spin to the soccer ball, as might happen for a free kick or a corner kick,[16] the ball may curve more than it would if it were not spinning. Forces associated with the spinning ball are usually parametrized by the Reynolds number and by the dimensionless spin parameter, Sp, which is the ratio of the rotating ball's tangential speed at the equator to its center-of-mass speed with respect to the air.[25] For a ball of radius r, angular speed ω, and center-of-mass speed v, Sp is given by

$$\mathrm{Sp} = \frac{r\omega}{v}. \tag{3}$$

Many student projects may be derived from our work because trajectory analysis can be done for many projected objects, not just soccer balls. Present-day software allows students to obtain sophisticated results without having to program complicated algorithms. We refer interested readers to Ref. 26 for the MATHEMATICA programs we wrote to analyze our trajectory data and to Ref. 27 for those wishing to learn about MATHEMATICA in the context of physics.

II. EXPERIMENTAL SETUP

We performed soccer ball launch experiments in a sports hall on the campus of the University of Sheffield. Figure 1 shows our ball launcher. Four counter-rotating wheels allow us to vary the launch speed and spin. Setting the four wheels independently at varying speeds allows balls to be fired with either no spin, topspin, backspin, sidespin, or a combination. Camera 1 was placed near the launcher to record the ball's launch. Figure 2 shows a schematic of our experimental setup. Camera 2 was used to record motion just before and past the ball's apex. We placed camera 2 against a wall so that the camera recorded as much of the trajectory as possible. We chose not to use a wide-angle lens with camera 2 because the ball images were too small in our videos. With our system there is a trade-off between ball size in the video and field of view. Camera 1 obtained roughly the first 0.07 s of the trajectory, and camera 2 obtained ≈0.4 s of the trajec-

Fig. 1. Ball launcher used for the trajectory experiments. Note the ball emerging from the launcher and the location of camera 1 on the right side of the photo.

Fig. 3. Data from camera 1 for a launch with no spin. The centers of the circles denote the ball's center of mass in 0.005 s intervals. The ball was launched with speed of $v_0 \simeq 18$ m/s at an angle of $\theta_0 \simeq 22°$ from the horizontal.

tory. Based on the launch speeds we used, the two cameras recorded the ball's trajectory during about one-third of its time in the air. Both high-speed cameras recorded at a rate of 1000 frames/s.

There are more elaborate and expensive experimental setups available, such as the HAWK-EYE system,[28] which is used in cricket, tennis, and, more recently, snooker. Our budget allowed the use of two quality high-speed cameras (~$2500 per camera). More sophisticated systems, which employ as many as six high-speed cameras for full three-dimensional data acquisition, are an order of magnitude more expensive than our system. Such systems are capable of tracking projected objects, although determining accurate rotation rates is still a challenge.

We also used markers on the ground to note the range of each launched ball. Based on visual observation of the landing positions, we estimate our range error to be no more than ± 5 cm.

CINE VIEWER[29] was used to convert a cine to AVI format. We did not notice any frame loss, a problem sometimes found when converting to AVI. Our software was used to track the ball and to obtain Cartesian coordinates of the ball's center of mass.[30] Figure 3 shows a sample of the data taken from camera 1. Figure 4 shows data taken from camera 2 of the launch shown in Fig. 3.

Once the data points were loaded into a file, the initial launch condition was obtained. The launch position is determined by measuring the height of the ball launcher's exit. The components of the initial velocity were determined using Richardson extrapolation,[31,32] which gives, among other results, a forward-difference expression for the first derivative using three points. If we want the derivative of a function $f(t)$ at t_0 and we know the value of $f(t)$ at t_0, t_1, and t_2, where $t_1 = t_0 + \Delta t$ and $t_2 = t_0 + 2\Delta t$ for a step size Δt, then the Richardson extrapolation gives for the first derivative at t_0

$$f'(t_0) \simeq \frac{-3f(t_0) + 4f(t_1) - f(t_2)}{2\Delta t}, \tag{4}$$

where the error is of order $(\Delta t)^2$.

The spin rate was determined by following a given point on the ball as the ball turned either a half turn (for slow spins) or a full turn (for fast spins). We achieved initial spin rates in the range from no spin to about 180 rad/s (more than 1700 rpm), though most tests were carried out for spin rates less than 125 rad/s.

III. FORCES ON BALL

The forces on projectiles moving through air have been discussed in many articles[33] and books.[34] Figure 5 shows the various forces on the ball. We assume the soccer ball's trajectory to be close enough to the surface of the Earth so that the gravitational force on the ball, $m\vec{g}$, is constant. The mass of the ball is $m = 0.424$ kg.

The air exerts a force on the soccer ball. The contribution to the air's force from buoyancy is small (~0.07 N) and is ignored. A scale used to determine weight will have that small force subtracted off anyway. The major contributions

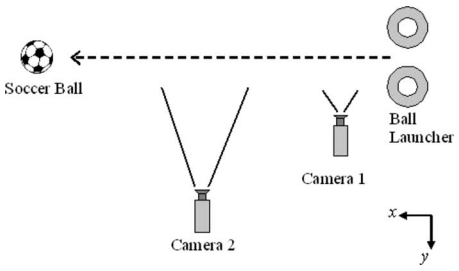

Fig. 2. A not-to-scale sketch of the experimental setup. Camera 1, about 1.5 m from the plane of the trajectory, records the launch of the soccer ball. Camera 2, about 13 m from the plane of the trajectory, records a portion of the trajectory near the apex of the flight. The z axis (not shown) points out of the page.

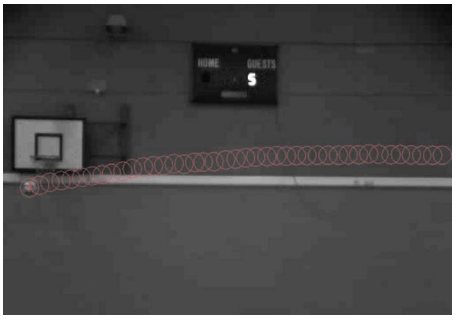

Fig. 4. Data from camera 2 for the no-spin launch in Fig. 3. Each circle's center notes the ball's center of mass in 0.010 s intervals. For more accurate results we zoom the image to four times what is shown. The ball landed 21.9 m from the launcher's base.

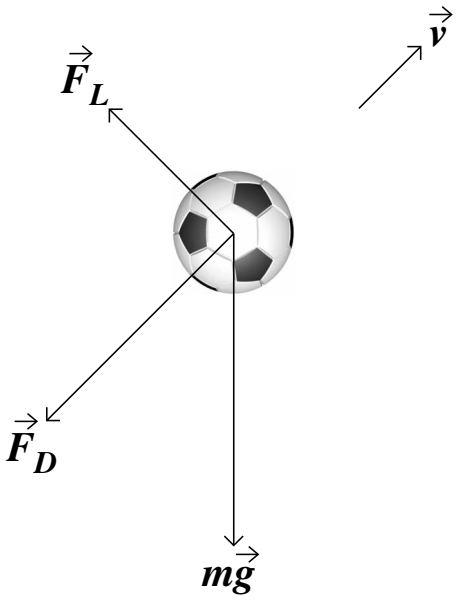

Fig. 5. The forces on a soccer ball. The gravitational force points down, the drag force is opposite the ball's velocity, the lift force is perpendicular to the ball's velocity and in the plane formed by the velocity and the ball's weight, and the sideways force (not shown) is into the page.

to the air's force come from resistive drag and the Magnus force. The drag force acts opposite to the ball's velocity, $\vec{v}$, and may be written as[35]

$$\vec{F}_D = \tfrac{1}{2}\rho A v^2 C_D(-\hat{v}), \tag{5}$$

where $\rho = 1.2\ \mathrm{kg/m^3}$ is the air density, $A \simeq 0.0375\ \mathrm{m^2}$ is the ball's cross-sectional area, $v = |\vec{v}|$ is the ball's speed, C_D is the dimensionless drag coefficient, and $\hat{v} = \vec{v}/v$.

Figure 6 shows wind-tunnel data from two experiments.[9,10] The experiments from Ref. 9 used two balls, a "scale" model (66 mm diameter), and a mini-soccer ball (140 mm diameter). Scale models are acceptable because two similar geometric objects will have the same drag coefficient for a given Reynolds number, a fact well known to aircraft designers. The wind-tunnel data from Ref. 10 were found using a regulation 32-panel ball, similar to our ball. Although there is slight disagreement over where the transition from laminar flow to turbulent flow occurs, both sets of data show the same qualitative feature, namely, a reduction in C_D by about a factor of 2 as the speed increases through the transition speed. We note that the scaled models used in Ref. 9 have sharper edges than real soccer balls, a fact that might explain the differences in data from Refs. 9 and 10.

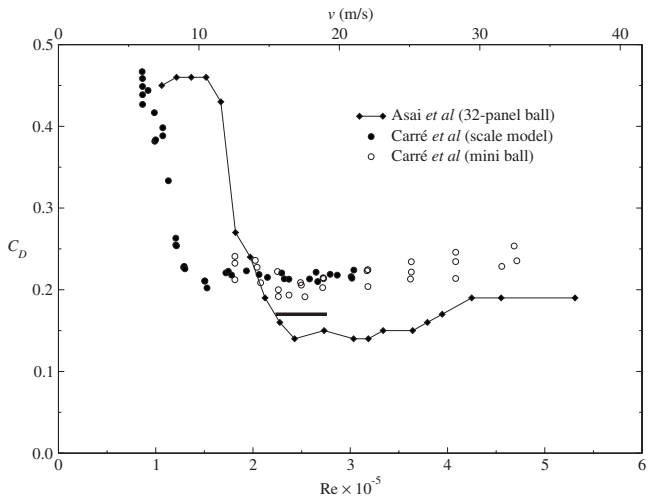

Fig. 6. Wind-tunnel data for C_D from Refs. 9 and 10. The Reynolds number is shown at the bottom, while the corresponding speed of a soccer ball is shown at the top. The line through the data from Ref. 10 is to help visually separate the two experiments. The thick line at $C_D = 0.17$ for $2.23 < \mathrm{Re} \times 10^{-5} < 2.76$ represents our maximum-speed launch.

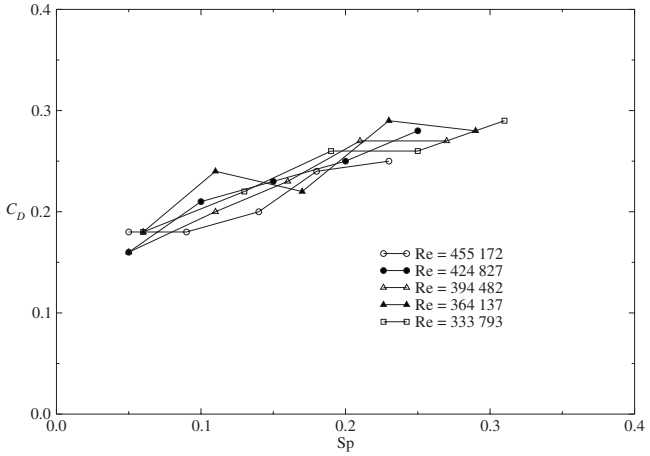

Fig. 7. Experimental wind-tunnel data from Ref. 10 for C_D as a function of Sp. Note that all five Reynolds numbers are above the transition. Lines between data points help to visually separate the five experiments.

Figure 7 shows wind-tunnel data[10] for C_D as a function of Sp. Note that all five post-transition tests show C_D values unaffected by changes in speed. As Sp increases, however, C_D increases.

The Magnus force arises when the ball spins while moving through the air. We refer the reader to Refs. 33 and 34 for quantitative discussions of the Magnus force. There are two components of the Magnus force that are relevant. The lift force, which points perpendicular to the drag force and remains in the plane formed by $\hat{v}$ and the ball's weight, is given by[36]

$$\vec{F}_L = \tfrac{1}{2}\rho A v^2 C_L \hat{\ell}, \tag{6}$$

where C_L is the dimensionless lift coefficient and $\hat{\ell}$ is a unit vector perpendicular to $\hat{v}$ and in the plane formed by $\hat{v}$ and the ball's weight.

The other component of the Magnus force is the sideways force given by[37]

$$\vec{F}_S = \tfrac{1}{2}\rho A v^2 C_S(\hat{\ell} \times \hat{v}), \tag{7}$$

where C_S is the dimensionless sideways coefficient. Because $\vec{F}_L$ and $\vec{F}_S$ arise from the same physical phenomena, finding C_L as a function of Reynolds number and spin parameter means also knowing C_S as a function of Reynolds number and spin parameter. We choose different subscripts for C_L and C_S because they are also functions of the spin axis direction. For pure topspin or backspin, $C_S = 0$; for pure sidespin, $C_L = 0$. Both C_L and C_S vanish if the rotational speed is zero (our model ignores "knuckle-ball" effects due to seam orientations). Our experimental approach is to work with either pure topspin or pure backspin. In such a case the motion

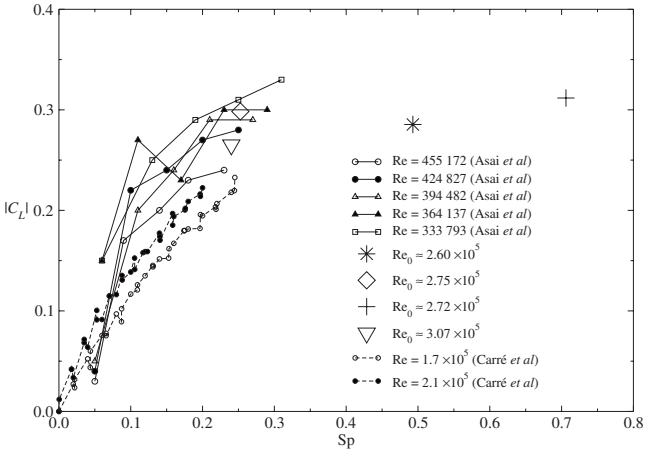

Fig. 8. Wind-tunnel data for $|C_L|$ from Refs. 9 and 10 as a function of Sp. Also shown are four data points from our trajectory analysis. The lines between data points visually separate the wind-tunnel data from our results.

is confined to two dimensions, and $C_S=0$. We determine C_L from the two-dimensional motion.

Figure 8 shows wind-tunnel data[9,10] for C_L as a function of Sp. Note that plotting C_L is the same as plotting C_S. We plot the absolute value of C_L because our C_L values are negative because the topspin created by our launcher produces a component of $\vec{F}_L$ pointing down. The plot shows that C_L increases in magnitude with increasing Sp.

We emphasize that the air exerts a single force on the ball. When we model the flight of the soccer ball, we need three components of the air's force because the ball moves in three dimensions. The drag, lift, and sideways forces are merely common choices used to model the air's force components.

Understanding the flight of a soccer ball requires knowledge of the dimensionless coefficients C_D, C_L, and C_S. Wind-tunnel experiments have yielded results over some of the range of Reynolds numbers and spin parameters associated with the game of soccer.

Incorporating the forces due to the air and gravity into Newton's second law gives

$$m\vec{a} = \vec{F}_D + \vec{F}_L + \vec{F}_S + m\vec{g}, \tag{8}$$

where $\vec{a}$ is the soccer ball's acceleration after it has left a player and before it hits anything. We use Eqs. (5)–(7) to write Eq. (8) as

$$\vec{a} = \beta v^2[-C_D\hat{v} + C_L\hat{\ell} + C_S(\hat{\ell}\times\hat{v})] + \vec{g}, \tag{9}$$

where $\beta=\rho A/2m \simeq 0.0530\ \text{m}^{-1}$.

Equation (9) is a second-order coupled nonlinear differential equation. After choosing a coordinate system, Eq. (9) must be solved numerically for the trajectory.

IV. MODEL IN TWO DIMENSIONS

Consider the case for which a soccer ball is launched with no sidespin so that $C_S=0$ in Eq. (9). It may have topspin, backspin, or no spin. The motion is thus confined to the x-z plane in Fig. 2. The unit vectors $\hat{v}$ and $\hat{\ell}$ are determined easily from Fig. 9 and are

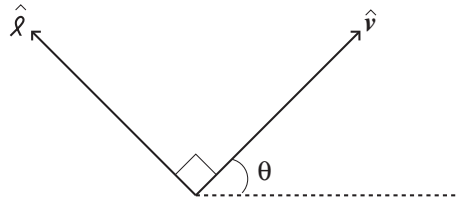

Fig. 9. The angle θ is the angle the velocity vector makes with the horizontal.

$$\hat{v} = \cos\ \theta\hat{x} + \sin\ \theta\hat{z} = \frac{v_x}{v}\hat{x} + \frac{v_z}{v}\hat{z}, \tag{10}$$

and

$$\hat{\ell} = -\sin\ \theta\hat{x} + \cos\ \theta\hat{z} = -\frac{v_z}{v}\hat{x} + \frac{v_x}{v}\hat{z}, \tag{11}$$

where v_x and v_z are the x and z components, respectively, of the velocity vector.

With $\vec{g}=-g\hat{z}$, Eq. (9) may be written as

$$a_x = -\beta v(C_D v_x + C_L v_z), \tag{12}$$

and

$$a_z = \beta v(-C_D v_z + C_L v_x) - g. \tag{13}$$

If the trajectory is known, the velocity and acceleration can be determined and Eqs. (12) and (13) may be solved for C_D and C_L, giving

$$C_D = -\left[\frac{(a_z+g)v_z + a_x v_x}{\beta v^3}\right], \tag{14}$$

and

$$C_L = \frac{(a_z+g)v_x - a_x v_z}{\beta v^3}, \tag{15}$$

where $v^2=v_x^2+v_z^2$. If we could determine exactly the trajectory from experiment and then find the velocity and acceleration from that trajectory, we could determine the drag and lift coefficients as functions of the speed. A major problem with this approach is that the numerical derivatives obtained from the experimental data have large errors associated with them.[38] We note that camera 1 records over a short enough time that we may obtain a reasonable estimate using Eqs. (14) and (15). For a sample of how this estimate is done using a simple spreadsheet, we refer the reader to Ref. 26. For those without MATHEMATICA, or for those looking for a simpler computational approach, we encourage downloading our EXCEL spreadsheet in Ref. 26.

V. MODEL IN THREE DIMENSIONS

We present our three-dimensional results for completeness. However, we have not developed a sophisticated tracking mechanism that allows us to obtain full three-dimensional trajectory data. Our ball launcher is capable of projecting soccer balls with sidespin. At present, we have codes[26] for a three-dimensional analysis. What we have done so far is to launch a ball with sidespin and note its landing point. From the horizontal and lateral ranges we can determine C_S assuming that it is constant over the trajectory. Given the wind-tunnel results in Fig. 8, such an assumption

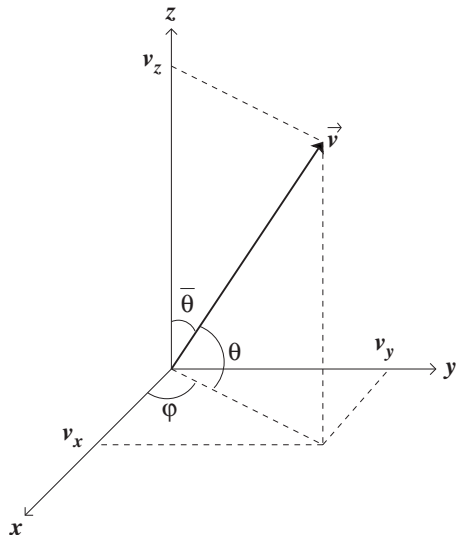

Fig. 10. The polar angle is $\bar{\theta}$, and the azimuthal angle is φ of the velocity vector. The angle measured from the horizontal is $\theta=\pi/2-\bar{\theta}$.

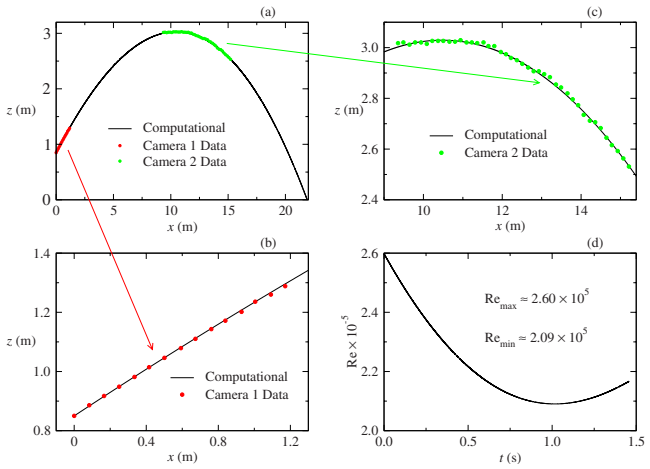

Fig. 11. (a) The computed trajectory using the initial launch conditions ($v_0 \simeq 18$ m/s and $\theta_0 \simeq 22°$) from the trajectory in Figs. 3 and 4. With $C_D=0.2$ and $C_L=C_S=0$, the computed range is 21.9 m. Also shown are the data points taken from cameras 1 and 2. (b) and (c) Zoomed-in portions of the parts of the trajectory recorded by cameras 1 and 2, respectively. The aspect ratio is not equal to one in the three trajectory plots. (d) The variation of the Reynolds number during the flight of the ball.

is not applicable, although C_S may not vary much. Improving our three-dimensional data acquisition is a goal of future work.

If a soccer ball possess sidespin, meaning that its spin axis is not perpendicular to the x-z plane in Fig. 2, $C_S \neq 0$ in Eq. (9). The ball thus moves in three dimensions instead of having its trajectory confined to the x-z plane. Figure 10 shows the velocity vector in three dimensions. The unit vector along $\vec{v}$ may be written as

$$\hat{v} = \sin\bar{\theta}\cos\varphi\hat{x} + \sin\bar{\theta}\sin\varphi\hat{y} + \cos\bar{\theta}\hat{z}, \tag{16}$$

or

$$\hat{v} = v_x\hat{x} + v_y\hat{y} + v_z\hat{z}. \tag{17}$$

The latter form will be more convenient for programming.

The unit vector $\hat{\ell}$ is found by taking $\hat{v}$ and rotating the angle $\bar{\theta}$ back by $\pi/2$ and keeping φ the same. Because $\sin(\bar{\theta}-\pi/2)=-\cos\theta$ and $\cos(\bar{\theta}-\pi/2)=\sin\theta$, the unit vector $\hat{\ell}$ is

$$\hat{\ell} = -\cos\bar{\theta}\cos\varphi\hat{x} - \cos\bar{\theta}\sin\varphi\hat{y} + \sin\bar{\theta}\hat{z}. \tag{18}$$

Figure 10 helps us to write the angles $\bar{\theta}$ and φ in terms of the Cartesian components of $\vec{v}$. From $\cos\bar{\theta}=v_z/v$ and $\tan\varphi=v_y/v_x$, we obtain $\sin\bar{\theta}=v_\perp/v$, $\cos\varphi=v_x/v_\perp$, and $\sin\varphi=v_y/v_\perp$, where $v_\perp=(v_x^2+v_y^2)^{1/2}$ and $v=(v_x^2+v_y^2+v_z^2)^{1/2}$. Equation (18) now becomes

$$\hat{\ell} = -\frac{v_x v_z}{v v_\perp}\hat{x} - \frac{v_y v_z}{v v_\perp}\hat{y} + \frac{v_\perp}{v}\hat{z}. \tag{19}$$

The third unit vector we need is $\hat{\ell}\times\hat{v}$. From Eqs. (16) and (18) we obtain

$$\hat{\ell}\times\hat{v} = -\sin\varphi\hat{x} + \cos\varphi\hat{y} = -\frac{v_y}{v_\perp}\hat{x} + \frac{v_x}{v_\perp}\hat{y}. \tag{20}$$

We substitute Eqs. (17), (19), and (20) into Eq. (9) and solve for the acceleration components to find

$$a_x = -\beta v\left(C_D v_x + \frac{C_L v_x v_z + C_S v v_y}{v_\perp}\right), \tag{21}$$

$$a_y = -\beta v\left(C_D v_y + \frac{C_L v_y v_z - C_S v v_x}{v_\perp}\right), \tag{22}$$

and

$$a_z = \beta v(-C_D v_z + C_L v_\perp) - g. \tag{23}$$

As we did in Sec. IV, we solve the acceleration component equations for the aerodynamic coefficients. The result is

$$C_D = -\left[\frac{(a_z+g)v_z + (a_x v_x + a_y v_y)}{\beta v^3}\right], \tag{24}$$

$$C_L = \frac{(a_z+g)v_\perp^2 - (a_x v_x + a_y v_y)v_z}{\beta v^3 v_\perp}, \tag{25}$$

and

$$C_S = \frac{a_y v_x - a_x v_y}{\beta v^2 v_\perp}. \tag{26}$$

Note that we recover our two-dimensional results if we set a_y, v_y, and C_S all to zero. As before, we can, in principle, determine the speed dependence of the aerodynamic coefficients from Eqs. (24)–(26). As discussed at the close of Sec. IV, using empirical data for numerical derivatives leads to velocity and acceleration components that are unreliable.

VI. RESULTS AND DISCUSSION

Figure 11 shows a typical no-spin trajectory. For no spin on the ball we set C_L and C_S both to zero and solve Eqs. (12) and (13) numerically for $x(t)$ and $z(t)$. The drag coefficient, C_D, is a free parameter. We minimized the square of the difference of the final value of x from the numerical solution with the measured range. C_D is varied until the computed range matches the experimentally measured range. The com-

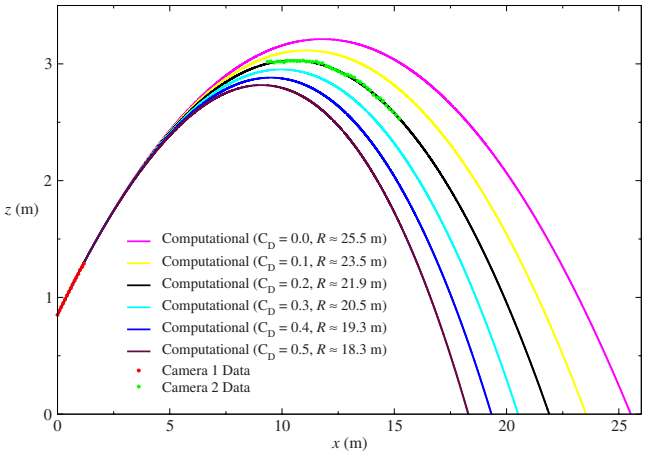

Fig. 12. The same plot as in Fig. 11(a), with numerical solutions for $0 \leq C_D \leq 0.5$. The value of the range R is given for each of the numerical solutions. The graph's aspect ratio is not equal to one.

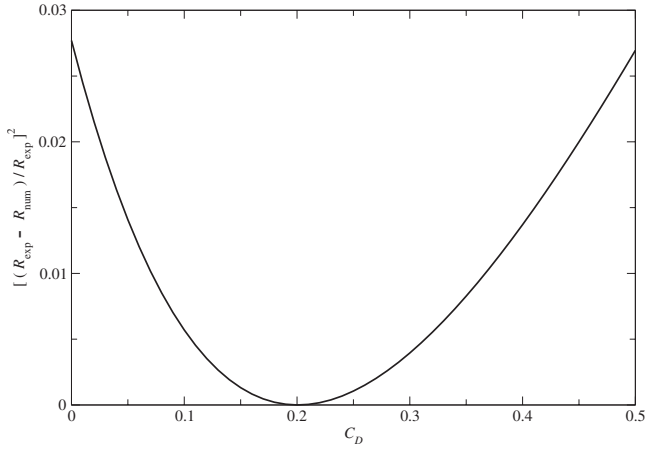

Fig. 13. The no-spin trajectory from Figs. 3 and 4 had an experimental range of $R_{exp} \simeq 21.9$ m. The plot shows how $[(R_{exp}-R_{num})/R_{exp}]^2$ varies with C_D, where R_{num} is the range determined from a numerical solution.

puted trajectory in Fig. 11 was made with $C_D=0.2$ and gave a range of 21.9 m, which was measured experimentally.

Also shown in Fig. 11 are the actual data points from the two cameras. The camera 1 data were shifted so that the first point matched the initial launch point. The camera 2 data were shifted so that the apex of the data matched the apex of the computational solution. Because the two cameras were not synchronized in time, we could not match the camera 2 data with the time points of the numerical solution. We determined the maximum height of the ball from the camera 2 data using a known length in the video. That maximum height matched the shifted camera 2 data's maximum height to two digits. The camera 2 data points do not sit perfectly on the numerical solution. Aside from small errors associated with trying to determine the center of the ball during the video analysis, the slightly erratic look to the data comes from knuckle-ball effects associated with a nonrotating ball.

Figure 11 also shows how the Reynolds number varies during the flight as determined from the numerical solution with $C_D=0.2$. The minimum value of Re is close to the transition region where turbulent flow changes back to laminar flow. Most of the flight takes place in the turbulent region.

To further demonstrate that our numerically determined value of C_D is accurate, we show in Fig. 12 that a value of C_D equal to 0.1 or 0.3 would have meant that the computed range would be off by $\approx$1.5 m from the 21.9 m we measured. An error of 1.5 m is an order of magnitude larger than the uncertainly associated with our range measurement. The difference in maximum heights between the $C_D=0.2$ curve and the $C_D=0.1$ or $C_D=0.3$ curves is about 10 cm. For a maximum height of $\approx$3 m an error of 10 cm is greater than the two-digit height accuracy we stated. A plot of the square of the difference between the experimental range and numerical ranges (normalized by the experimental range) is shown in Fig. 13. We thus believe that the recorded trajectory seen in Figs. 3 and 4 corresponds to a trajectory with $C_D=0.2$.

The initial launch speed of $\approx$18 m/s corresponds to Re $\simeq 2.6\times 10^5$, meaning that the ball was launched well past the transition speeds predicted by both wind-tunnel experiments. The C_D value we found is for a post-transition launch Reynolds number that is just past the Reynolds number where the wind-tunnel data from Ref. 9 cross the wind-tunnel data from Ref. 10 (see Fig. 6). To sort out which experimental data we are matching, we launched a ball at the maximum speed that we could obtain without hitting the ceiling rafters or the far wall. A launch speed of $\approx$19.4 m/s, corresponding to Re $\simeq 2.76\times 10^5$, is the maximum speed we could test, given our sports hall and launcher. Such a launch speed gave an experimental range of 24.6 m. We did the same analysis used to create Figs. 11–13 and obtained $C_D=0.17$ for our maximum-speed launch. This C_D value is slightly closer to the Ref. 10 data, which are the one we expect to match, given that the Ref. 10 measurement used a regulation sized soccer ball. Unfortunately, our facilities do not allow us to launch a nonspinning ball fast enough to obtain post-transition data at higher Reynolds numbers. From our numerical solution the minimum Reynolds number for our maximum-speed launch trajectory is Re $\simeq 2.23\times 10^5$. Because we assume a constant value of C_D in our numerical solution, we include in Fig. 6 our results using $C_D=0.17$ for the range of $2.23\times 10^5 <$ Re $< 2.76\times 10^5$.

For rotating balls we can extract values of C_L from camera 1 data only. The reason is that the Reynolds number and spin parameter do not change appreciably during the $\approx$0.07 s from the launch that camera 1 records. For the ranges of launch speeds and spins we used, we surmised from both cameras that the ball's spin rate decreases around 4%–8% by the time the ball had just passed its flight apex. Previous work suggests that spin decay is roughly exponential.[39] We assume that the spin rate has dropped by about 10% by the time the ball hits the ground and that the maximum decrease in speed (and thus Re) is roughly 20%, as seen in Fig. 11(d). Because Sp increases as Re decreases, we expect C_L to increase in magnitude throughout the ball's flight based on the wind-tunnel data in Fig. 8.

Figure 14 shows four sets of camera 1 data, each with the corresponding numerical solution. The latter was generated by choosing the appropriate C_D from Fig. 7 (extrapolating if necessary), meaning C_D is no longer a free parameter, and then optimizing the numerical solution to give the least-squares deviation from the data points. The position data points come from taking a single launch video, analyzing it on three separate occasions, and then averaging the three sets of results. Despite the fact that the three sets of data are in quantitative agreement, we find that the averaging signifi-

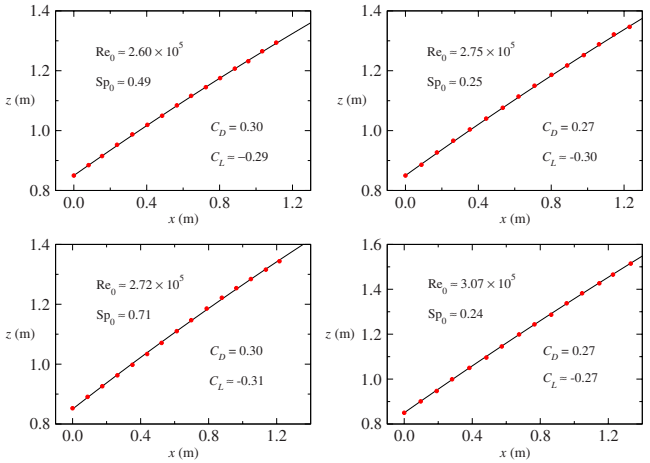

Fig. 14. Four experiments with soccer balls launched with topspin. Initial values of Re and Sp are shown. Values of C_D chosen for the numerical solutions are also shown with the corresponding numerically generated C_L values.

cantly reduces errors that we introduce when identifying the ball's center of mass in each frame of the video analysis. All four launches had topspin, meaning that the lift force has a downward component, which is why C_L is negative. As we vary C_D by $\pm 30\%$, the change in C_L is less than 5%, which implies that if we are a little off in our estimate of C_D from Fig. 7, our C_L values will not be very sensitive to errors.

We have included the C_L results from Fig. 14 in Fig. 8. Note that our two points for $\mathrm{Sp} \simeq 0.25$ are within the experimental data from Ref. 10. Our contribution verifies previous wind-tunnel work[10] and adds two new points for values of Sp that have not been reported from existing wind tunnels. Our results suggest a possible leveling off of the magnitude of C_L as Sp increases. We plan to do more experiments at large spin parameters. For a ball of radius r with center-of-mass speed v and rotation speed ω, the speed of one side of the ball with respect to the air is $v+r\omega$, and the relative speed on the opposite side is $v-r\omega$. That means that the relative speed of the latter of these two sides can be smaller than the transition speed. For $\mathrm{Sp}=1$ the speed of the ball with respect to the air on the $v-r\omega$ side would be zero. We thus do not expect the lift coefficient data to follow the near linear trends suggested by the wind-tunnel data shown in Fig. 8.

Professional soccer players are capable of producing remarkable trajectories when taking spot kicks, such as the famous goal by David Beckham in the World Cup Qualifiers for England against Greece in 2001. Our analysis of time-coded television footage of this free kick indicates that the ball left Beckham's foot at about 36 m/s ($\mathrm{Re} \simeq 5.1 \times 10^5$) from about 27 m away from the goal. He imparted an average of $\omega \simeq 63$ rad/s ($\mathrm{Sp} \simeq 0.19$) on the ball. It rose above the height of the crossbar during its flight and moved laterally about 3 m, before slowing down to about 19 m/s ($\mathrm{Re} \simeq 2.7 \times 10^5$) as it dipped into the corner of the goal.

We can do a back-of-the-envelope calculation to estimate the aerodynamic coefficient needed to produce the bend in Beckham's kick. We assume that the speed of the kick is constant and equal to the average speed ($\sim$27.5 m/s), the spin is pure sidespin, and the only sideways force is described by Eq. (7). These assumptions are not correct but are reasonable enough to estimate C_S. The time of flight is roughly $t \simeq (27\ \mathrm{m})/(27.5\ \mathrm{m/s}) \simeq 0.98$ s. The sideways acceleration, a_S, can be estimated by assuming constant acceleration, giving $3\ \mathrm{m} \simeq (1/2) a_S t^2$. The result is $a_S \simeq 6.2\ \mathrm{m/s^2}$, which implies that the sideways force is $ma_S \simeq 2.6$ N. If we equate the magnitude of Eq. (7) with this force and use the estimate of the average speed, we obtain $C_S \simeq 0.2$. From the experimental results near $\mathrm{Sp}=0.19$ in Fig. 8 and the fact that C_S and C_L arise from the same physical phenomena, we see that our estimate for C_S is reasonable.

The real work to find aerodynamic coefficients needs to be done in wind tunnels or in a manner similar to what we have described in this paper.

ACKNOWLEDGMENTS

We wish to thank the two referees for valuable suggestions for improving our paper.

[1] Lyman J. Briggs, "Effects of spin and speed on the lateral deflection (curve) of a baseball; and the Magnus effect for smooth spheres," Am. J. Phys. **27**, 589–596 (1959).
[2] E. Achenbach, "Experiments on the flow past spheres at very high Reynolds numbers," J. Fluid Mech. **54**, 565–575 (1972).
[3] E. Achenbach, "The effects of surface roughness and tunnel blockage on the flow past spheres," J. Fluid Mech. **65**, 113–125 (1974).
[4] Robert G. Watts and Eric Sawyer, "Aerodynamics of a knuckleball," Am. J. Phys. **43**, 960–963 (1975).
[5] Robert G. Watts and Ricardo Ferrer, "The lateral force on a spinning sphere: Aerodynamics of a curveball," Am. J. Phys. **55**, 40–44 (1987).
[6] P. W. Bearman and J. K. Harvey, "Golf ball aerodynamics," Aeronaut. Q. **27**, 112–122 (1976).
[7] S. J. Haake, S. G. Chadwick, R. J. Dignall, S. Goodwill, and P. Rose, "Engineering tennis—Slowing the game down," Sports Eng. **3**, 131–144 (2000).
[8] R. D. Mehta and J. M. Pallis, "Sports ball aerodynamics: Effects of velocity, spin and surface roughness," in *Materials and Science in Sports*, edited by F. H. Froes and S. J. Haake (TMS, Warrendale, PA, 2001), pp. 185–197.
[9] M. J. Carré, S. R. Goodwill, and S. J. Haake, "Understanding the effect of seams on the aerodynamics of an association football," J. Mech. Eng. Sci. **219**, 657–666 (2005).
[10] T. Asai, K. Seo, O. Kobayashi, and R. Sakashita, "Fundamental aerodynamics of the soccer ball," Sports Eng. **10**, 101–110 (2007).
[11] Sarah Barber, "The aerodynamics of association footballs," Ph.D. thesis, University of Sheffield, July 2007.
[12] M. A. Passmore, S. Tuplin, A. Spencer, and R. Jones, "Experimental studies of the aerodynamics of spinning and stationary footballs," J. Mech. Eng. Sci. **222**, 195–205 (2008).
[13] M. J. Carré, T. Akatsuka, and S. J. Haake, "The curve kick of a football: II. Flight through the air," Sports Eng. **5**, 193–200 (2002).
[14] John Wesson, *The Science of Soccer* (Institute of Physics, Bristol, 2002).
[15] K. Bray and D. G. Kerwin, "Modelling the flight of a soccer ball in a direct free kick," J. Sports Sci. **21**, 75–85 (2003).
[16] Brandon G. Cook and John Eric Goff, "Parameter space for successful soccer kicks," Eur. J. Phys. **27**, 865–874 (2006).
[17] John Eric Goff, *Gold Medal Physics* (Johns Hopkins U. P., Baltimore, MD, 2010), Chap. 7.
[18] Joseph M. Zayas, "Experimental determination of the coefficient of drag of a tennis ball," Am. J. Phys. **54**, 622–625 (1986).
[19] Antonin Štěpánek, "The aerodynamics of tennis balls—The topspin lob," Am. J. Phys. **56**, 138–142 (1988).
[20] LeRoy W. Alaways and Mont Hubbard, "Experimental determination of baseball spin and lift," J. Sports Sci. **19**, 349–358 (2001).
[21] Alan M. Nathan, "The effect of spin on the flight of a baseball," Am. J. Phys. **76**, 119–124 (2008).
[22] Frank M. White, *Fluid Mechanics*, 6th ed. (McGraw-Hill, New York, 2008), p. 27.
[23] Reference 22, pp. 476–480.
[24] We used a standard 32-panel soccer ball manufactured by Umbro, model X III 250.

[25] D. J. Tritton, *Physical Fluid Dynamic*, 2nd ed. (Clarendon, Oxford, 1988), pp. 159–161.
[26] The programs at ⟨http://goff-j.web.lynchburg.edu/MathematicaAJP.html⟩ are free for readers to download and modify as they wish.
[27] Robert L. Zimmerman and Fredrick I. Olness, *MATHEMATICA for Physics*, 2nd ed. (Addison-Wesley/Prentice-Hall, San Francisco, 2003).
[28] See ⟨www.hawkeyeinnovations.co.uk⟩ for more information.
[29] CINE VIEWER by Phantom may be downloaded for free at ⟨www.visionresearch.com/index.cfm?page=software⟩. Note that a "cine" is simply a motion picture.
[30] Our in-house software was developed by Richard Dignall and Simon Goodwill at the University of Sheffield. There are other commercially available software packages that allow one to analyze trajectories from videos. A good one sold primarily in the U.S. is VIDEOPOINT.
[31] John H. Mathews, *Numerical Methods for Computer Science, Engineering, and Mathematics* (Prentice-Hall, London, 1987), p. 284.
[32] Kendall E. Atkinson, *An Introduction to Numerical Analysis* (Wiley, New York, 1989), p. 317.
[33] See, for example, R. D. Mehta, "Aerodynamics of sports balls," Annu. Rev. Fluid Mech. **17**, 151–189 (1985).
[34] See, for example, Neville De Mestre, *The Mathematics of Projectiles in Sports* (Cambridge U. P., Cambridge, 1990).
[35] Reference 34, p. 39.
[36] Reference 34, p. 105.
[37] Reference 34, p. 106. Note that we write the cross product in the opposite way that De Mestre does.
[38] See, for example, Ref. 31, pp. 281–283, and Ref. 32 pp. 318–320.
[39] David James and Steve Haake, "The spin decay of sports balls in flight," in *The Engineering of Sport 7*, edited by M. Estivalet and P. Brisson (Springer, Paris, 2008), Vol. 2, pp. 165–170.

Standard Volumes. I suspect that most colleges had collections of vessels of standard volumes at the turn of the twentieth century, but, since they do not look like scientific apparatus, they have vaporized. This set of eight copper standard volume measures at the left at Kenyon College range from two liters to one centiliter. The maker is unknown, but many apparatus manufacturers sold them. For example, an identical set in tinned iron sold for $2.00 in the 1912 catalogue of the V. H. Stoelting Co. of Chicago. (Photograph and Notes by Thomas B. Greenslade, Jr., Kenyon College)